

Article

Effect of Process Temperature on the Texture Evolution and Mechanical Properties of Rolled and Extruded AZ31 Flat Products

Maria Nienaber ^{1,*} , Gerrit Kurz ¹, Dietmar Letzig ¹, Karl Ulrich Kainer ²  and Jan Bohlen ¹

¹ Institute of Material and Process Design, Helmholtz-Zentrum Hereon GmbH, Max-Planck-Str. 1, 21502 Geesthacht, Germany

² Light Elements Engineering, Foundry and Automation, Wrocław University of Science and Technology, Wyspińskiego 27, 50-370 Wrocław, Poland

* Correspondence: maria.nienaber@hereon.de

Abstract: The application of magnesium flat products is affected by the limited formability at room temperature and the anisotropy of the mechanical properties. The main reason for this is the underlying hexagonal crystal structure of magnesium and the development of strong crystallographic textures during massive forming processes with distinct alignment of basal planes. For an improvement in the properties of semi-finished products, the detailed knowledge of the influence of the manufacturing process on the microstructure and texture evolution of the flat products as a result of dynamic and static recrystallization is required. In this work, flat products made of conventional magnesium alloy AZ31 were manufactured by the rolling process as well as by direct extrusion, with variation in the process temperature. This allowed the development of a distinct variation in microstructures and textures of the flat products. The effects on mechanical properties and formability are highlighted and discussed in relation to the microstructure and texture. It is shown that both the process and the temperature have a major influence on texture and consequently on the material properties.

Keywords: magnesium; rolling; extrusion; flat products; texture; formability; mechanical properties; AZ31



Citation: Nienaber, M.; Kurz, G.; Letzig, D.; Kainer, K.U.; Bohlen, J. Effect of Process Temperature on the Texture Evolution and Mechanical Properties of Rolled and Extruded AZ31 Flat Products. *Crystals* **2022**, *12*, 1307. <https://doi.org/10.3390/cryst12091307>

Academic Editor: Shouxun Ji

Received: 31 August 2022

Accepted: 13 September 2022

Published: 16 September 2022

Publisher's Note: MDPI stays neutral with regard to jurisdictional claims in published maps and institutional affiliations.



Copyright: © 2022 by the authors. Licensee MDPI, Basel, Switzerland. This article is an open access article distributed under the terms and conditions of the Creative Commons Attribution (CC BY) license (<https://creativecommons.org/licenses/by/4.0/>).

1. Introduction

There has been extended research activity in the field of magnesium and its alloys for more than two decades associated with a continuously increasing demand based on weight-specific characteristics (density 1.74 g/cm³) and good castability for structural lightweight metallic applications. The aim is still to develop cast and wrought Mg alloys with superior properties and excellent processability [1,2]. The goal is to improve mechanical properties such as creep resistance, ductility and specific strength through adjusted thermomechanical processing and alloy design strategies.

Up to now, in comparison to cast parts, flat products made of wrought alloys have only been used to a limited extent. This can be attributed to the poor formability of wrought Mg alloys, which results from the crystallographic hexagonal close-packed (HCP) structure of magnesium. In addition, the massive deformation process during rolling or extrusion of flat magnesium products leads to the development of a pronounced crystallographic deformation texture [3–5] with distinct alignment of the basal planes parallel to the forming direction. As the critical shear stress (CRSS) for basal slip is much lower than that for non-basal slip systems and the activation of other slip systems at room temperature is restricted [6–11], Mg alloys with a strong texture and distinct alignment of basal planes exhibit poor plastic formability at RT. The existence of a pronounced crystallographic orientation leads also to mechanical anisotropy and premature failure of the material. To solve

this problem, researchers have reported that a reduction in grain size as well as a weakening of the basal texture can significantly improve the mechanical behavior [12–15]. Studies on the Mg alloy AZ31 suggested that the predominant deformation mechanisms at low temperatures are basal slip and tensile twinning. During the massive deformation process, this often leads to the development of the above mentioned strong basal texture [16–19]. While many research approaches offered texture weakening concepts by adding specific alloying elements (such as rare earth elements or Ca) and by their influence on the deformation and recrystallization behavior [4,20–22], the massive forming process itself also has a significant effect on the development of the microstructure. Extrusion is a one-step forming process, which includes that the degree of deformation is significantly higher than in the case of rolling. Studies have shown that the degree of deformation has an influence on the recrystallization behavior, which usually results in a smaller grain size and a decreasing texture intensity [23,24]. During rolling, less dynamic recrystallization (DRX) is observed, but static recrystallization (SRX) during intermediate heat treatment determines the microstructure development, whereas in extrusion DRX is the predominant mechanism for microstructure development. However, a certain SRX effect can also be present if the extrusion is carried out at very high temperatures followed by air-cooling. Consequently, the resulting texture development is influenced by the impact of such different recrystallization mechanisms. Furthermore, the process parameters during rolling [25–29] and consequently also during extrusion [4,30–36] have a significant influence on the recrystallization behavior.

The goal of this research is to show the impact of the manufacturing process, and consequently the deformation and recrystallization mechanisms, on the texture and microstructure development for AZ31. Therefore, flat products were produced by the conventional rolling process to analyze the SRX as well as produced by the direct extrusion process to investigate the DRX. In addition, the impact of the processing temperature on the microstructure development is studied with respect to the different recrystallization mechanisms in rolling and extrusion. The effects on mechanical properties and formability are highlighted and discussed in relation to the microstructure and texture.

2. Materials and Methods

For this study, extrusion billets and rolling slabs were machined from industrially produced AZ31 ingots (3 wt% Al, 1 wt% Zn, 0.4 wt% Mn). The ingots were manufactured by gravity die casting. The billets (length 75 mm, diameter 49 mm) and the slabs (50 mm length, 95 mm width, 17 mm thickness) were homogenized in an air-driven furnace (Nabertherm GmbH, Lilienthal, Germany) without protective gas at 400 °C for 16 h and then air-cooled before the experiments.

The directly extruded magnesium bands were produced using a 2.5 MN automatic extrusion press with a container diameter of 50 mm (Müller Engineering GmbH, Todtenweis, Germany). A die with an inlet angle of 45° and a gap width of 40 mm × 2 mm was used, which corresponds to an extrusion ratio of 1:24.5. The extrusion temperature was increased from 200 °C to 500 °C in 50° steps, with a constant extrusion speed of 0.6 mm/s for all experiments. The billets were preheated in an air-driven furnace (Nabertherm GmbH, Lilienthal, Germany) without protective gas for 60 min to the extrusion temperature. After the experiment, the bands were air-cooled to room temperature.

A duo cold rolling mill (type 205; maximum applied rolling force 50 t; Metz Industrie-Design GmbH, Schöneck, Germany) was used for the rolling experiments. The homogenized slabs were rolled in 14 passes to a final thickness of 1.4 mm. The first 4 rolling passes were performed with a deformation degree of 0.1, the following 9 passes with 0.2 and the final pass with 0.3. The same rolling schedule has been applied in earlier work and is an well-established rolling plan, which has proven to avoid early fracture of the rolling slabs [37]. Before the first rolling pass, the rolling slabs were heated to the rolling temperature in an air-driven furnace without using protective gas for 30 min. After each subsequent rolling pass, an intermediate annealing of 15 min was performed at the rolling temperature. After the final pass, the rolled sheets were air-cooled. The sheets produced

had a length of about 550 mm and a width of about 110 mm. The rolling speed remained constant at ca. 16 m/min for all trials. Rolling experiments with rolling temperature at 400 °C, 450 °C and 500 °C were carried out. Recrystallization annealing of the rolled sheets was performed at 450 °C for 10 min.

The grain structure and texture of the flat products were analyzed by using a field emission scanning electron microscope (SEM) combined with electron backscatter diffraction (EBSD), Zeiss Crossbeam 550 L (SEM, Ultra 55, Carl Zeiss AG, Oberkochen, Germany). An accelerating voltage of 15 kV and a step size of 0.4 µm at 600× magnification were used. The samples for this purpose were polished using a LectroPol-5 (Struers™) electropolishing machine with AC2 solution electrolyte (Struers™) at −20 °C and a voltage of 30 V for 30–60 s (condition and alloy dependent). To remove the oxidation layer, the samples were rinsed with 0.1% nitric acid. Data analysis was performed using TSL OIM software (version 7, EDAX, Mahwah, NJ, USA).

For the tensile tests in longitudinal and transverse direction (according to DIN 50125), a universal testing machine Z050 with a maximum load of 50 kN (Zwick GmbH & Co.KG, Ulm, Germany) was used. The dog-bone-shaped samples were machined to a gauge length of 18 mm and a width of 5 mm. For statistical validation, at least 3 specimens were tested at room temperature with a constant initial strain rate of 10^{-3} s^{-1} until failure of the samples. The change in length of the specimen was recorded using a mechanical extensometer. Stress–strain diagrams were prepared from the recorded data and the mechanical properties were determined. The stretch-forming behavior was investigated by using Erichsen tests (type 145-60, Erichsen GmbH & Co.KG, Hemer, Germany) (according to DIN EN ISO 20482) with a lubricant (OKS 352) at room temperature. The punch diameter was 20 mm, the forming speed (punch displacement) was 5 mm/min and the blank holder force was 10 kN.

3. Results

3.1. Microstructure and Texture Development

Figure 1 shows the microstructure of the investigated sheets and texture in the form of inverse pole figure (IPF) maps with orientation-dependent color code as well as the corresponding (0001) and (10–10) pole figures. Figure 1a represents the sheets in the as-rolled condition after rolling with different slab temperatures and Figure 1b shows the same sheet after a heat treatment of 10 min at 450 °C. In the as-rolled condition, all microstructures show a highly deformed structure visible by the intragranular orientation variations. The average grain size increased with the rolling temperature from 11 to 17 µm. After the heat treatment, a fully recrystallized (no intragranular orientation variations), fine-grained, globular microstructure was found in all cases, with an average grain size of 13 to 21 µm.

The corresponding texture measurements show a weakening of the maximum intensity of the (0002) pole figure with an increase in the rolling temperature from 400 °C to 500 °C. This is visible in both conditions, the as-rolled sheets and the heat-treated sheets, while the heat treatment itself results in a visible texture weakening. The sheets in the as-rolled condition after rolling at 400 °C and 450 °C, respectively, show a basal texture in the (0002) pole figures in the form of a $\langle 0001 \rangle$ fiber parallel to the normal direction (ND) ($\langle 0001 \rangle // \text{ND}$) with the broadest angular tilt of basal planes to the rolling direction (RD). This type of texture is characteristic for AZ31 sheets. The basal planes are mainly oriented parallel to the sheet surface (c-axis parallel to the ND) and the prismatic planes are randomly distributed perpendicular to the ND. At 500 °C, a splitting of the basal planes towards the RD can be seen. In addition, a significant increase in the tilting angle of the basal planes to the transverse direction (TD) was also found.

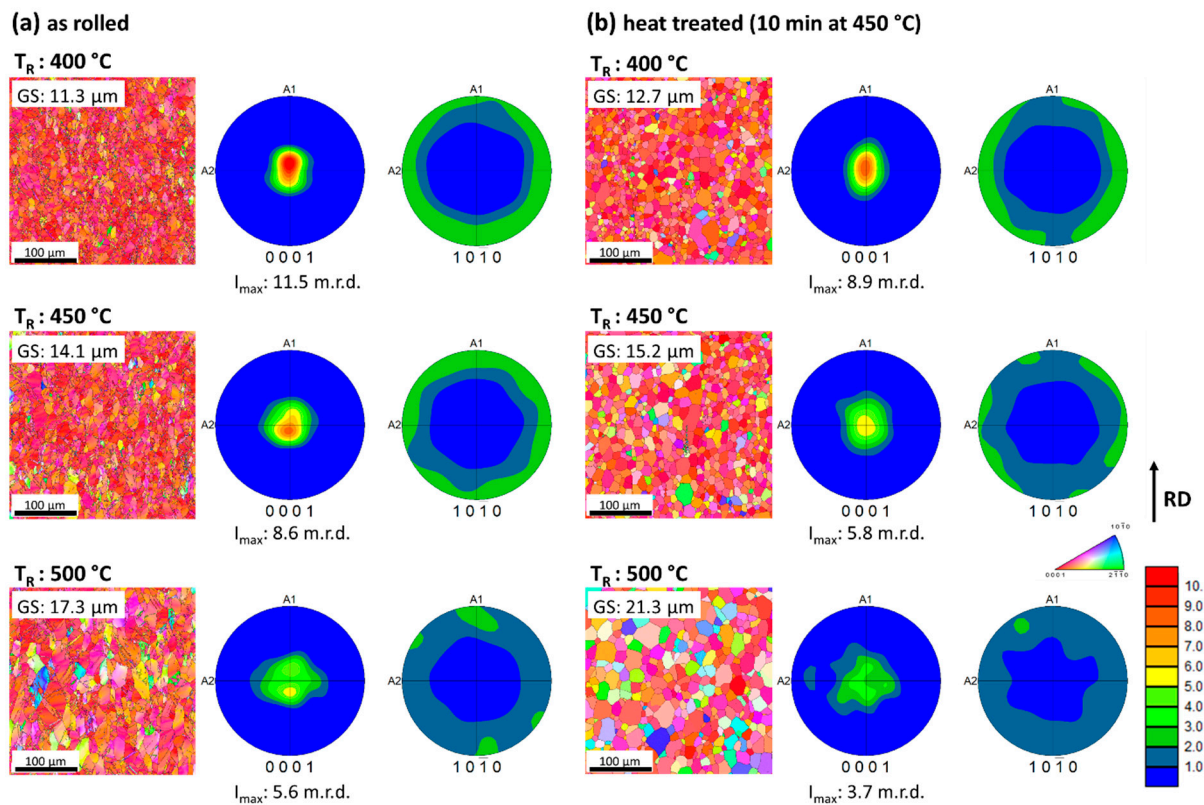


Figure 1. Inverse pole figure maps of AZ31 sheet (a) as-rolled, (b) after heat treatment for 10 min at 450 °C.

After the heat treatment and regardless of the rolling temperature, the (0002) pole figure reveals a basal component and a $\langle 0001 \rangle$ // ND fiber with a broader angular distribution to the RD direction rather than to the TD. The annealed sheet rolled at 500 °C shows very weak split peaks of the basal planes and a broader angular distribution in the TD direction. This condition exhibited the lowest maximum intensity of the (0002) pole figure among the AZ31 sheets, with 3.7 m.r.d.

The inverse pole figure maps (IPF) for extruded flat bands are shown in Figure 2 for the applied extrusion temperature ranges between 200 °C and 500 °C. At low temperatures, a bimodal globular microstructure with non-recrystallized grains elongated parallel to the extrusion direction (ED) is observed. An increasing extrusion temperature results in an increase in the recrystallized fraction of the microstructure, although elongated grains are still maintained. It is visible that the microstructure development changes if the extrusion temperature exceeds 400 °C. A completely recrystallized microstructure with a clear grain growth can be seen. In addition, the grain structure has a less globular nature. This means that the grains are clearly elongated longitudinally to the extrusion direction.

The corresponding texture development of the extruded bands shows clear differences compared to the rolled AZ31 sheets in Figure 1. At an extrusion temperature of 200 °C, a strong basal texture ($I_{\max} = 8.8$ m.r.d.) with a $\langle 0002 \rangle$ fiber parallel to the normal direction is observed. Additionally, the basal planes have a broader angular distribution to ED rather than to the TD. With increasing extrusion temperature, a $\{0001\} \langle 10\bar{1}0 \rangle$ component becomes clearly visible identified with the six-peaks appearance in the (10 $\bar{1}0$) pole figure. After extrusion at 400 °C or higher temperatures, also a weak $\langle 10\bar{1}0 \rangle$ fiber parallel to the extrusion direction ($\langle 10\bar{1}0 \rangle$ // ED) is indicated by basal planes more tilted to the TD and two strong intensity peaks along ED in the (10 $\bar{1}0$) pole figure. This prismatic fiber becomes more pronounced at even higher extrusion temperatures. In addition to this pronounced $\langle 10\bar{1}0 \rangle$ fiber // ED, there is another $\{10\bar{1}0\} \langle 11\bar{2}0 \rangle$ component visible which

is represented by strong intensity poles in \pm TD in the (0002) pole figure and equivalently by the three intensity poles in the (10 $\bar{1}$ 0) pole figure.

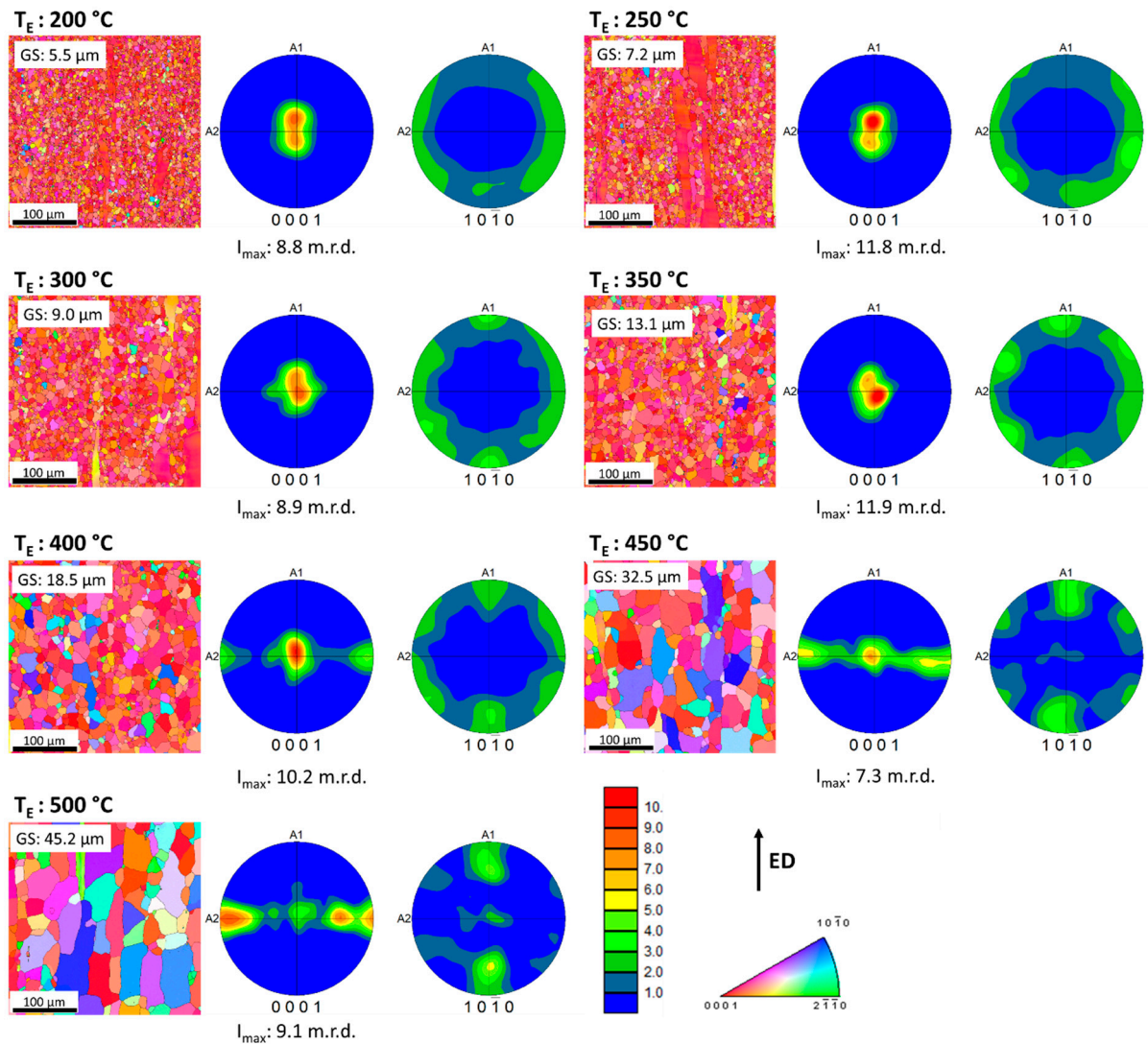


Figure 2. Inverse pole figure maps of the extruded AZ31 bands.

3.2. Mechanical and Forming Behavior

Figure 3 shows the engineering stress–strain curves of the as-rolled and annealed sheets. The graphs of that specimen were selected that most closely reflect the averaged values, shown in Tables 1 and 2. In the as-rolled condition, a typical curve for a work-hardened material is shown with rather high yield stresses, no significant additional increase in the stress to the tensile strength and low uniform and low fracture elongation in the range of 0.5–4.7%. With an increase in the rolling temperature, a decrease in strength is observed. After rolling at $400\text{ }^\circ\text{C}$ and $450\text{ }^\circ\text{C}$, TYS and UTS are higher for the transverse direction rather than for the rolling direction. In contrast, after a rolling temperature of $500\text{ }^\circ\text{C}$, the TYS along the rolling direction with 236 MPa is significantly higher compared to TYS in the transverse direction with 188 MPa.

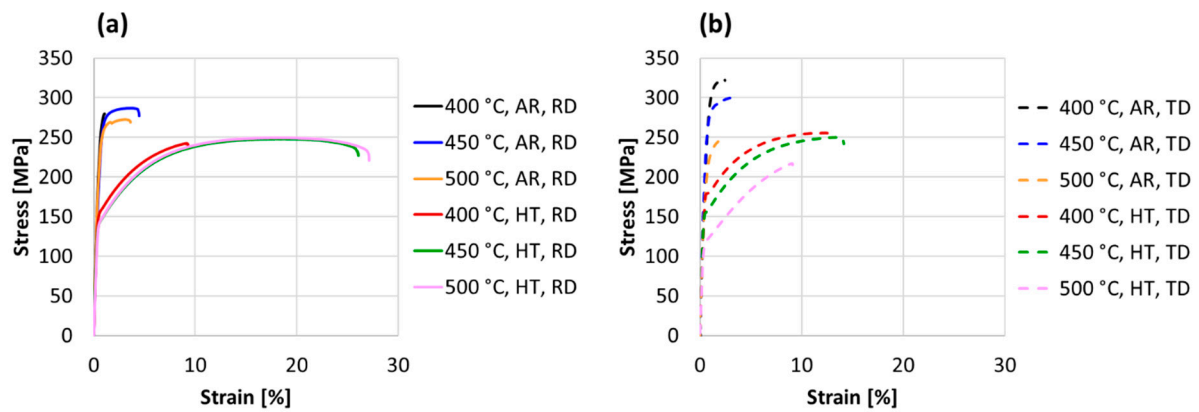


Figure 3. Engineering stress–strain diagram in (a) RD and (b) TD from the sheets in as-rolled (AR) and heat-treated (HT) condition.

Table 1. Tensile properties at room temperature of the as-rolled sheets tested along RD, TD (TYS, tensile 0.2% yield stress; UTS, ultimate tensile stress, ϵ_u , uniform elongation; ϵ_f , elongation to fracture).

T_R (°C)		TYS (MPa)	UTS (MPa)	ϵ_u (%)	ϵ_f (%)	Erichsen Value (mm)	Grain Size (μm)
400	RD	246 ± 2	267 ± 27	0.5 ± 0.3	0.5 ± 0.3	2.0 ± 0.1	11.3
	TD	273 ± 5	320 ± 11	2.1 ± 1.3	2.3 ± 1.5		
450	RD	249 ± 8	287 ± 2	2.8 ± 1.3	3.4 ± 1.9	2.5 ± 0.2	14.1
	TD	235 ± 23	302 ± 8	3.8 ± 2.8	4.7 ± 3.5		
500	RD	236 ± 8	275 ± 10	3.5 ± 3.2	4.2 ± 3.9	3.0 ± 0.4	17.3
	TD	188 ± 6	248 ± 7	2.1 ± 1.5	2.3 ± 1.8		

Table 2. Tensile properties at room temperature of the heat-treated sheets tested along RD, TD (TYS, tensile 0.2% yield stress; UTS, ultimate tensile stress; ϵ_u , uniform elongation; ϵ_f , elongation to fracture).

T_R (°C)		TYS (MPa)	UTS (MPa)	ϵ_u (%)	ϵ_f (%)	Erichsen Value (mm)	Grain Size (μm)
400	RD	153 ± 1	243 ± 1	6.2 ± 5.3	6.4 ± 5.5	3.0 ± 0.2	12.7
	TD	178 ± 1	255 ± 3	11.2 ± 2.6	12.1 ± 3.2		
450	RD	143 ± 1	247 ± 3	17.1 ± 1.3	12.3 ± 4.6	4.8 ± 0.4	15.2
	TD	155 ± 1	250 ± 1	12.2 ± 0.8	13.1 ± 0.6		
500	RD	124 ± 1	233 ± 10	14.6 ± 5	17.2 ± 7.3	6.1 ± 0.3	21.3
	TD	116 ± 2	216 ± 1	8.2 ± 0.4	8.3 ± 0.5		

Subsequent annealing of the sheets results in a typical decrease in yield strength and tensile strength. Additionally, a significant increase in elongation is observed, obviously a result of softening the sheets based on static recrystallization and a concurrent decrease in the dislocation density. The rolling-temperature-dependent development of the mechanical properties of the heat-treated sheets is comparable to those in the as-rolled condition. With the increase in the rolling temperature, there is a decrease in UTS and TYS. The heat-treated sheet after rolling at 500 °C shows a higher yield strength in the rolling direction (124 MPa) than the transverse direction (116 MPa). The ductility in the rolling direction increases considerably with an increase in the rolling temperature from 6.4 to 17.2%.

The stress–strain curves of the extruded bands are shown in Figure 4. Again, only one representative sample is shown for each condition, which most closely represents the averaged mechanical properties (see Table 3). The extruded material shows a typical behavior for ductile materials throughout. Following a continuous elasto–plastic transition, plastic material behavior becomes apparent. The curves in ED and TD show a clear orientation dependence, which are well-known for magnesium flat products [38]. The anisotropic material behavior is especially pronounced in the yield strength (TYS) for extrusion temperatures above 400 °C. At an extrusion temperature of 200 °C, the material has a yield strength of 165 MPa in ED and 203 MPa in TD. While the yield strength in ED is almost constant for all extrusion temperatures (TYS (T_E : 450 °C): 168 MPa), a drop of 110 MPa to 93 MPa can be observed in TD at 200 °C. The influence of the texture and microstructure on the mechanical behavior is highly demonstrated in this case. The variation in strength (UTS) (Table 3) of the material is almost independent of the process temperature and testing direction. A slight decrease from 275 MPa in ED and 279 MPa in TD at 200 °C to 248 MPa in ED and 246 MPa in TD at 500 °C is observed. Elongation at failure reveals no change in ED (20.1% to 19.9%) but a marked decrease in TD (24.6% to 13.2%) with an increase in process temperature from 200 °C to 500 °C.

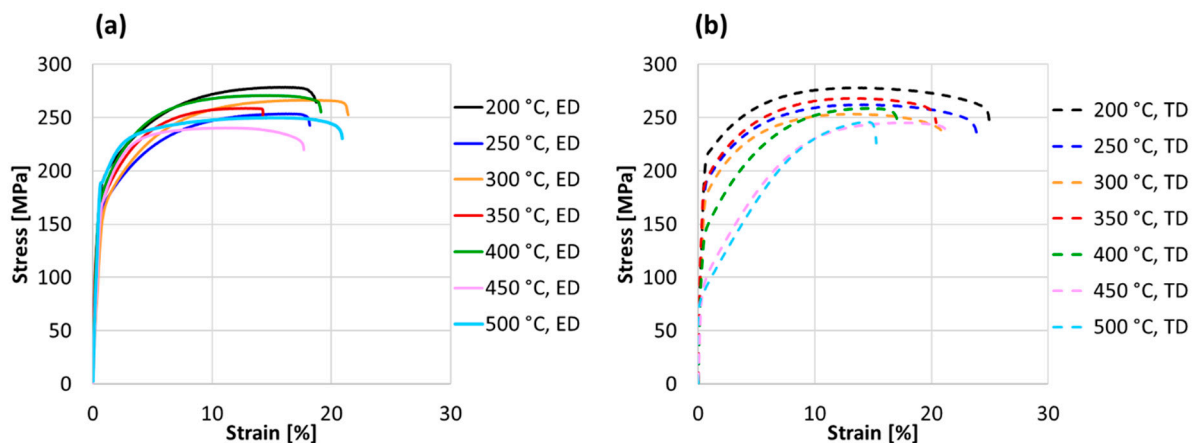


Figure 4. Engineering stress–strain diagram in (a) ED and (b) TD from the extruded flat bands.

Erichsen cupping tests were carried out to investigate the biaxial forming behavior at room temperature. The presented curves in Figure 5 reveal an increase in the force after attaching the punch to the sample surface and the beginning of the deformation while forming the cup. The drawing path is then shown as the resulting depth of the formed cup. The force increase is continued until a sudden drop due to sample fracture. The maximum drawing distance up to the drop in force is referred to as the Erichsen value (IE). Average values are collected in Tables 1–3.

For the extruded bands (Figure 5b), no difference in the slope of the curve can be observed. Thus, there is no change in the hardening behavior and no significant variation in the Erichsen value. Minimal increase to 3.4 mm with increasing temperature to 500 °C can be noticed. For the rolled sheets (Figure 5a), there is a pronounced impact of the rolling temperature and of the additional heat treatment on the Erichsen value. At the lowest rolling temperature without subsequent heat treatment, the specimens have the steepest increase in force values compared to the other conditions. This can be correlated with a high work hardening during rolling, because of the low rolling temperature. In addition, it can be correlated with the results from the tensile tests of the as-rolled sheets (Figure 3). Here, a distinct trend in a change of UTS with an increase in rolling temperature from 400 °C through 450 °C to 500 °C is shown.

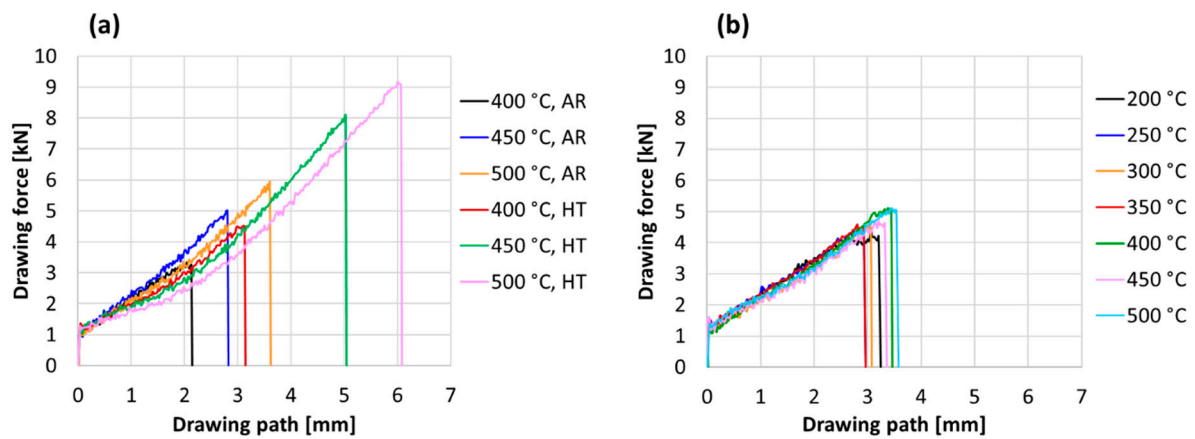


Figure 5. Drawing force—drawing path curves from Erichsen cupping tests at room temperature for (a) rolled sheets and (b) extruded bands.

Table 3. Tensile properties at room temperature of the extruded bands tested along ED, TD (TYS, tensile 0.2% yield stress; UTS, ultimate tensile stress; ϵ_u , uniform elongation; ϵ_f , elongation to fracture).

T_R (°C)		TYS (MPa)	UTS (MPa)	ϵ_u (%)	ϵ_f (%)	Erichsen Value (mm)	Grain Size (μm)
200	ED	165 ± 4	275 ± 5	15.9 ± 0.4	20.1 ± 3.6	3.2 ± 0.5	5.5
	TD	203 ± 5	279 ± 1	12.9 ± 0.4	24.6 ± 1.3		
250	ED	148 ± 3	259 ± 5	15.0 ± 0.8	17.3 ± 1.6	2.9 ± 0.1	7.2
	TD	185 ± 1	262 ± 1	13.6 ± 0.5	23.2 ± 0.3		
300	ED	157 ± 9	264 ± 5	16.4 ± 0.7	19.6 ± 2.7	3.0 ± 0.1	9.0
	TD	171 ± 5	250 ± 6	12.8 ± 0.3	21.1 ± 0.5		
350	ED	153 ± 5	262 ± 2	12.3 ± 1.3	14.1 ± 2.8	2.8 ± 0.1	13.1
	TD	180 ± 4	268 ± 1	13.3 ± 1.1	20.5 ± 1.0		
400	ED	169 ± 5	272 ± 3	13.9 ± 0.3	18.5 ± 0.5	3.3 ± 0.2	18.5
	TD	137 ± 2	255 ± 4	14.0 ± 0.2	16.6 ± 0.4		
450	ED	168 ± 7	238 ± 2	11.2 ± 1.2	16.7 ± 0.6	3.2 ± 0.1	32.5
	TD	93 ± 2	242 ± 6	16.9 ± 0.6	20.6 ± 0.4		
500	ED	184 ± 5	248 ± 2	14.4 ± 0.1	19.9 ± 0.3	3.4 ± 0.3	45.2
	TD	86 ± 1	246 ± 1	12.8 ± 0.1	13.2 ± 0.4		

In the as-rolled condition, a slight increase in Erichsen value from 2.0 mm to 3.0 mm can be seen with an increase in rolling temperature from 400 °C to 500 °C. In contrast, the heat-treated sheets reveal a significant increase in the Erichsen value. After heat treatment, the sheet rolled at 400 °C has an IE of 3 mm, whereas the sheet rolled at 500 °C shows an Erichsen value of 6.1 mm, which is an increase by a factor of two. This condition also shows the lowest slope in the increase in the force value, but the highest force value is reached when the material fails. In correlation to the tensile properties for the heat-treated sheets (Figure 3), a distinct trend in the change in elongation with an increase in rolling temperature from 400 °C to 450 °C is indicated.

4. Discussion

4.1. Texture Development

For the AZ31 sheets, a typical basal texture was observed, which could be described by a preferential orientation of the basal planes parallel to the sheet plane. Generally, the basal texture is caused by the activity of basal $\langle a \rangle$ slip [5,16]. With an increase in rolling temperature, a weakening of the texture intensity (11.5 to 5.6 m.r.d.) occurs as well as a splitting of the preferred position of the basal planes into two poles with deflection to the rolling direction.

Huang et al. [39,40] explain the texture weakening during rolling with increasing process temperature by the increase in the relative proportion of non-basal slip mechanisms, which inhibits the formation of a strict orientation of the basal planes parallel to the sheet plane. High-temperature rolling produces a high density of non-basal dislocations, which induces a rotation of the c -axis orientation, resulting in the development of the visible double peak. This leads to a weakening of the basal alignment. The formation of the split peak with tilt to the rolling direction, which is also clearly found in the AZ31 sheet rolled at 500 °C, is associated with active $\langle c + a \rangle$ slip [41].

Along with basal slip, twinning is the easiest deformation mechanism to activate. For AZ31 sheets, Guo et al. [26] suggest that twinning is the predominant deformation mechanism during hot rolling with a small thickness reduction. This indicates that twinning has a significant influence on texture formation, with considerable reorientation of twinned grain fractions. In both mechanisms (basal slip and twinning), the activation ability proceeds athermally, i.e., there is no pronounced influence of the temperature increase [42,43].

However, for the AZ31 sheets rolled in this study, a clear influence of the rolling temperature on the twin fraction can be observed. This is illustrated in Figure 6 by the indexing of the twin boundaries in sections of EBSD measurements and the distribution diagram of the misorientation angles. It is noteworthy that the as-rolled condition of the sheets enables the investigation of active deformation mechanisms due to the low fraction of the DRXed microstructure.

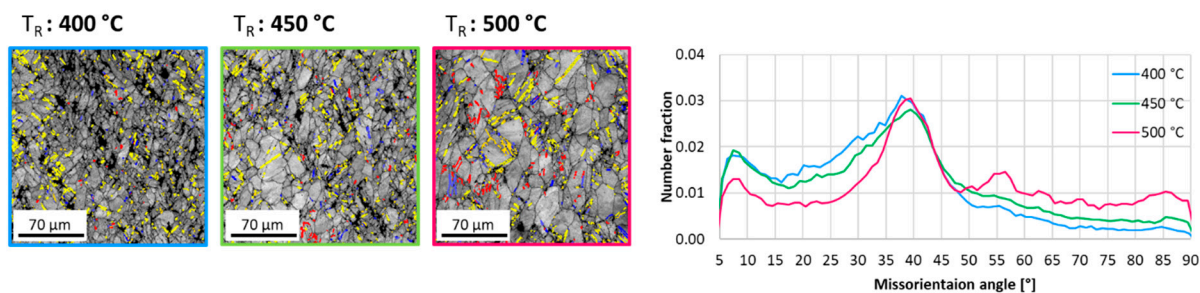


Figure 6. Indexing of the twin boundaries (compression twins (blue), tension twins (red), double twins (yellow)) in the sections from EBSD measurements and misorientation angle distribution of the as-rolled sheets.

The different types of twins are highlighted in color. The frequency of the misorientation angles shows the fraction of different twin modes in the microstructure. Tension and compression twins differ visually. Tensile twins occupy large areas in the deformed grains, formed by lateral growth during deformation [42]. In contrast, compression twins appear as the thin areas in the grain typical of deformation twins. Secondary twinning occurs within an already twinned region.

The $\{10\text{--}11\} + \{10\text{--}12\} \langle 1\text{--}210 \rangle$ double twins (38°, yellow) appear as the most prevalent twin variant regardless of the rolling temperature. No significant difference is seen between a rolling temperature of 400 °C and 450 °C. The as-rolled condition at 500 °C exhibits, in addition to the $\{10\text{--}11\} - \{10\text{--}12\}$ double twins, an increased fraction of $\{10\text{--}11\} \langle 1\text{--}210 \rangle$ compression twins (56°, red) and $\{10\text{--}12\} \langle 1\text{--}210 \rangle$ tension twins (86°, blue). The largest fraction is attributable to the double twins and the smallest to the compression twins, indicating that most of the compression twins were converted to double

twins by subsequent tensile twinning. As the process temperature increases, a coarsening of the twins becomes visible. This correlates with grain coarsening with increasing rolling temperature. This grain coarsening takes place during annealing between rolling passes.

Since the mechanical twinning is considered to be independent of the process temperature, consequently athermal [44–46], the larger proportion of tensile and compressive twins, at high rolling temperature, is initially not explicable. When a strain component perpendicular to the c-axis occurs during rolling, {10–12} tensile twins can be more easily activated in grains with a tilted c-axis [47]. Furthermore, using rolled AZ31 sheets with different grain sizes, Azghandi et al. [48] showed that grain refinement leads to a lower twin area fraction. Hence, it appears worthwhile to assume that the increasing grain size promotes twinning and the twin growth. According to this, the microstructure development at high rolling temperature leads to a certain grain coarsening with a rather weak basal texture, which favors an increased activation of twinning systems during the following hot rolling passes. Twinning may reduce stress concentration due to plastic incompatibilities at grain boundaries and reduce stored strain energy.

Figure 7 shows the corresponding grain orientations of the parent grains and different kinds of twins for the sheet rolled at 500 °C. It becomes clear that especially the compression and tension twins lead to a broader distribution of the grain reorientations (texture weakening). The double twins lead only to a slight tilting of the orientation in the rolling direction. This preferential twinning results in a significant texture weakening with an increase in rolling temperature, as can be seen from Figure 1.

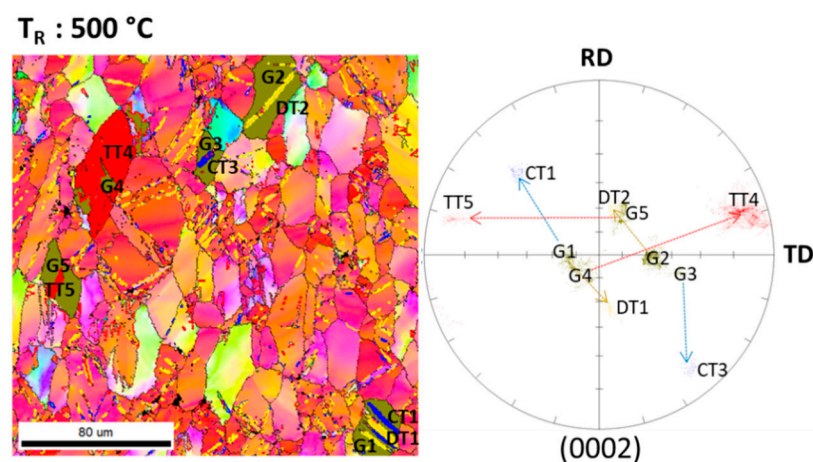


Figure 7. Twin orientations for an AZ31 sheet rolled at 500 °C. Green: parent grains (G1–G5); red: tension twins (TT4, TT5); blue: compression twins (CT1, CT3); yellow: double twins (DT1, DT2).

The subsequent heat treatment of the sheets also has an influence on texture development. The development of the recrystallization texture depends on the orientation distribution in the underlying deformation texture (activity of the deformation mechanisms). Here, the twins can have a significant effect on texture development and more concretely on texture weakening. This was demonstrated in a previous work [20] for a rolled sheet based on a Mg–Zn–Ca alloy. A significant texture weakening due to a randomization of the orientation distribution has been explained by locally pronounced twin reorientations

As shown in Figure 1, the subsequent heat treatment of the rolled AZ31 sheet leads to a significant weakening of the texture. The increased number of twins at higher temperature, especially tensile twins, results in significant texture weakening at 500 °C from 5.5 to 4.0 m.r.d. compared to at 400 °C from 9.4 to 9.1 m.r.d. and a higher tilt angle to the TD. Earlier studies have shown [20,49] that twins and twin boundaries serve as dominant nucleation sites during static recrystallization of Mg alloys, which can explain the significant texture weakening with an increased twin fraction. This can also be demonstrated in this research, as shown in Figure 7.

While in rolling the static recrystallization is predominant for the microstructure and texture development, for extrusion the dynamic recrystallization is the prevailing recrystallization mechanism. For the extruded AZ31 bands (see Figure 2), as the temperature increases, there is a development from a basal $\{0001\}$ $\langle 10\text{--}10 \rangle$ component with a $\langle 0001 \rangle // \text{NR}$ fiber to a prismatic $\{10\text{--}10\}$ $\langle 11\text{--}20 \rangle$ component with pronounced $\langle 10\text{--}10 \rangle // \text{SR}$ fiber. At an extrusion temperature below 400°C , such as in the rolled AZ31, the basal components dominate the texture with the c-axis oriented perpendicular to the band plane.

In Figure 8a the microstructure for the band extruded at 200°C is distinguished into fractions by using grain orientation spread (GOS) as a separator. Grains with low orientation spread are assumed to be the result of a grain nucleation and growth mechanism during recrystallization [20,50]. On the other hand, grains that have undergone active dislocation glide tend to have a broader range of orientations. In this work, a separation of both fractions, assumed to represent a recrystallized and a non-recrystallized fraction of the microstructure, is based on a constraint of $\text{GOS} = 1^\circ$. For the non-recrystallized fraction of the microstructure ($\text{GOS} > 1^\circ$), the $\{0001\}$ $\langle 10\text{--}10 \rangle$ component dominates the (0002) pole figure. For the recrystallized grains ($\text{GOS} < 1^\circ$), a rotation of 30° around the c-axis occurs, and accordingly the $\{0001\}$ $\langle 11\text{--}20 \rangle$ component is more present. This component is also dominating the texture with increased process temperatures up to 400°C (see Figure 2). These kinds of basal components and fibers are typical for AZ31, and a slight splitting of the basal poles in the extrusion direction is also characteristic [18,51–53]. The formation of the basal components occurs due to the basal $\langle a \rangle$ -slip system along the given deformation direction, which results in an alignment of the basal planes in the band plane [41,54,55]. Splitting of the basal pole in the direction of deformation has been attributed to the activity of pyramidal $\langle c + a \rangle$ -slip [18,56] or to double twins, as is the case for the rolled sheets.

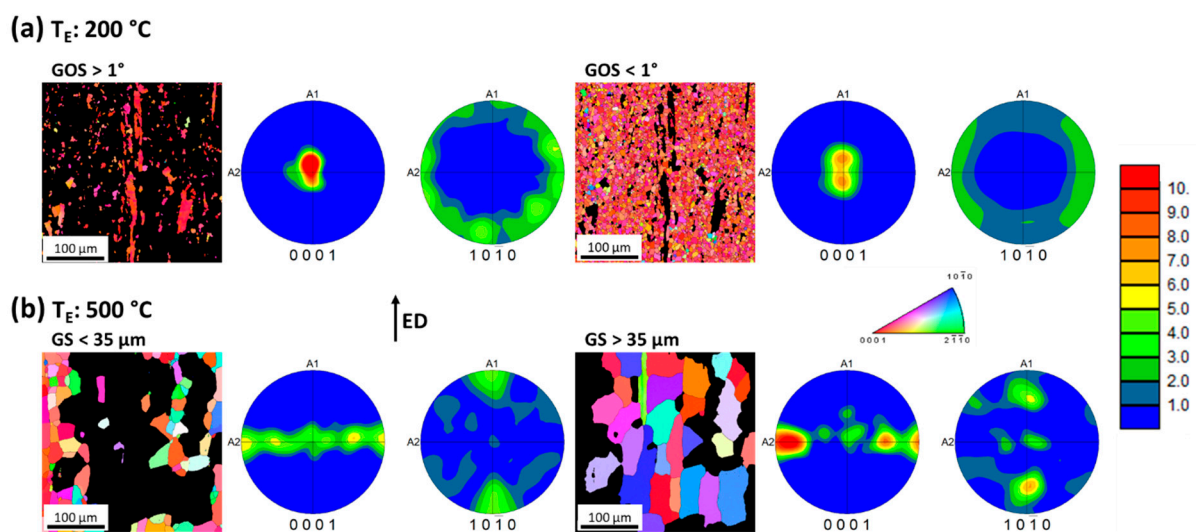


Figure 8. EBSD measurement of AZ31: (a) extruded at 200°C separated by grain orientation spread (GOS); (b) extruded at 500°C separated by the grain size (GS).

The extrusion temperature-dependent evolution of the texture shows that, in contrast to rolling, the basal components do not dominate the (0002) pole figure at all temperatures. At higher extrusion temperatures, 400°C and above, a prismatic component or fiber is formed. Grains with a c-axis parallel to the band or grains with basal planes tilted in TD occur more frequently.

In Figure 8b, this situation is shown for an extrusion temperature of 500°C . The larger grains (grain size (GS) $> 35 \mu\text{m}$) tend to have a higher tilt angle in the transverse direction than the smaller grains (GS $< 35 \mu\text{m}$). Thus, the dominance of the $\{10\text{--}10\}$ $\langle 11\text{--}20 \rangle$ component is dependent on the dynamic grain growth, where this orientation is formed by a preferential grain growth.

Imandoust et al. [57] and Tang et al. [58] attributed the formation of the prismatic component to higher activity of prismatic slip. On the other hand, Jiang et al. [3] suggested that prismatic slip is not the main reason for the basal plane alignment, but the variations in basal texture could be mainly attributed to twinning and subsequent continuous (cDRX) and discontinuous (dDRX) dynamic recrystallization behavior during extrusion, which are related to the deformation conditions such as temperature and strain. Using directly extruded AZ31 round bars, Jiang et al. [3] show that both {10–11} compression and {10–12} tensile twins are active in the early stage of extrusion. Different types of compression twins resulted in the corresponding grains being realigned toward non-fiber orientation and further led to the formation of the {10–10} fiber component with the help of basal $\langle a \rangle$ - and prismatic $\langle a \rangle$ -slip. No DRX occurred inside the compression twins, but these twins facilitated the subsequent cDRX process by accommodating and realigning the original grains. Conversely, tensile twins became active with increasing strain in the original grains. The twinning-induced DRX mechanism triggered the nucleation of fine DRX grains with non-basal orientation in the tensile twins, but only contributed to the overall texture development to a limited extent. This finding by Jiang that the cDRX forms the prismatic component or prismatic fiber fits the results of the microstructure analysis of the extruded AZ31 bands (see Figure 2). Here, it was observed that with increasing extrusion temperature, the globularity of the microstructure decreases significantly. As reported by Yi et al. [17], dDRX produces mainly globular grains, while cDRX decreases the globularity and the grain shape tends to be more longitudinally stretched in the extrusion direction.

Thus, the microstructure finding correlates with the texture development based on cDRX. In addition, Fatemi-Varzaneh et al. [59] reported that at temperatures above 450 °C and low strain rates cDRX is predominating the microstructure development. In addition, for RE-containing Mg alloys it can be shown [4] that cDRX dominated the microstructural development during extrusion and led to a (10–10) basal fiber orientation.

However, since multiple mechanisms are expected to interact, it is plausible to assume that, in addition to cDRX, a higher proportion of active prismatic sliding also leads to the formation of the {10–10} $\langle 11\text{--}20 \rangle$ component or the $\langle 10\text{--}10 \rangle$ // SR fiber.

4.2. Microstructure–Property Correlation

The strength of metals generally increases with decreasing grain size due to grain boundary strengthening. One criterion for the onset of plastic flow is the yield strength, since the yield strength is determined by an influence of the dislocation mobility in a polycrystalline material.

Figure 9 shows the Hall–Petch relationship, the dependence of yield strength on grain size, for the rolled and heat-treated sheets and the extruded bands in the longitudinal and transverse directions. The shape of the curve, in particular its slope, represents the hardening of the material caused by the grain size, unless any other influencing variables, such as texture or the degree of recrystallization, have to be taken into account. A difference in the yield strength in the longitudinal and transverse directions indicates an anisotropic material behavior, which is often attributable to a distinct texture.

For the as-extruded band in the extrusion direction (yellow line), almost no grain size dependence on the tensile yield stress is visible. In the transverse direction (red line), the coarse-grained material tends to show the Hall–Petch relationship, but in the fine-grained material, as in ED, there is no dependence on the grain size. The sheets in as-rolled condition show a clear Hall–Petch relationship in TD (black line) but not in RD (green line). Moreover, at 450 °C the anisotropy is reversed. In addition, for the heat-treated rolled sheets, the Hall–Petch relation is the most likely, but here again the yield strength isotropy is turned around. By considering the results of the Hall–Petch plot, it is possible to exclude the grain size argument from the discussion of possible mechanisms, since the dependencies show that orientation of the grains (texture), not grain size, is clearly found to be the dominating factor for the yield strength. For this reason, the influence of the texture on the yield strength and its anisotropy are discussed in the following.

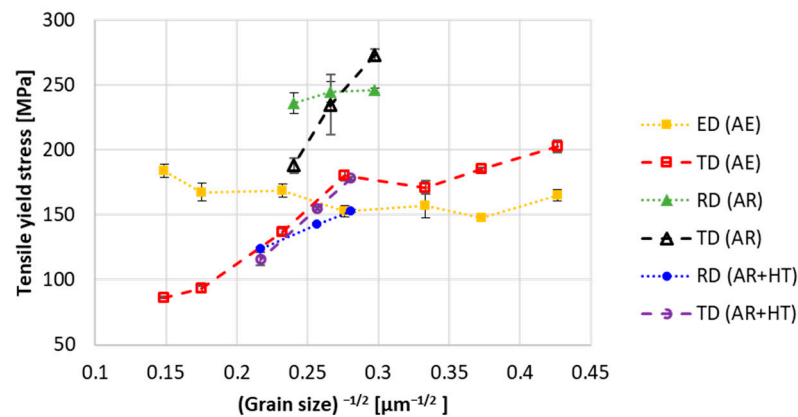


Figure 9. Tensile yield stress parallel to ED or RD and TD from tensile tests vs. the inverse square route of the average grain size (Hall–Petch plot): AE (as-extruded), AR (as-rolled), HT (heat-treated).

At a rolling temperature of 400 °C and 450 °C (Figure 1), respectively, and at the extrusion temperatures of 200 °C to 350 °C (small grains) (Figure 2), the basal texture of the rolled and heat-treated sheets, as well as the extruded bands, features a slight spreading of the basal pole along the rolling direction or extrusion direction. In these cases, the yield strength shows a higher value along the transverse direction than along the rolling direction/extrusion direction. The slight tilt of the basal plane along the band plane increases the Schmid factor for basal slip, thus facilitating the ability to activate basal slip [38]. This consideration follows Schmid’s law, which describes the critical shear stress required to move the dislocations on the most closely packed planes. Even this slight asymmetry of the base pole in the (0002) pole figure leads to a noticeable anisotropy of the yield strength, as it has also been described in [60].

A slight variation in texture can also explain the reversal of the anisotropy of the rolled and heat-treated sheets at a rolling temperature of 500 °C. Due to the angular spreading of the basal planes in the transverse direction at high temperatures of the as-rolled and heat-treated sheets and the associated easier activation of basal slip, the reversal in anisotropy (decrease in yield strength in TD) can be justified with this.

Especially significant becomes the influence of texture on the anisotropy of the yield strength for extrusion temperatures of 400 °C to 500 °C (coarse grains). Due to the formation of a prismatic fiber and/or a prismatic component in the (0002) pole figure, there is a pronounced decrease in the yield strength in the transverse direction (TD) of the extruded bands (Figure 9, red line). For this type of texture, the {10–12} <10–11> tensile twins can also contribute to the deformation, since the c-axis of some grains is parallel to the tensile stress, here in TD. This leads to a lower yield strength because twinning induces plastic deformation at an early stage. However, twinning leads to strong geometrical strengthening due to interactions of dislocations with twin grain boundaries, as well as reorientation of the crystal lattice (c-axis in twin grains almost perpendicular to the load axis). As a result, high tensile strengths can be achieved in ED (Figure 9, yellow line). The increase in yield strength in ED can of course also be justified by the small angular broadening of the basal plane in ED.

Due to a small angular broadening (strong basal orientation), the material will also be more difficult to undergo plastic deformation, as it is more difficult to activate basal slip. Consequently, texture is instrumental in determining the anisotropy of the material. This is in agreement with results of Agnew et al. [41]. They showed on a weak texture that basal slip is particularly active. This mechanism determines the strengthening capacity of the material. An increase in the activity of basal slip causes a decrease in strain hardening ability and results in higher elongation, and high elongation is required for high biaxial deformation. Thus, the preferred activity of basal slip (texture) determines the yield strength and its anisotropy.

The correlation between texture (maximum intensity of the (0002) pole figure) and the Erichsen value for the flat products produced at the different process temperatures are shown in Figure 10. A weak texture is necessary for a high formability. As shown in the figure, this does not always fit. For AZ31 in the as-rolled condition, this behavior is evident, but for the extruded material, no real tendency can be seen.

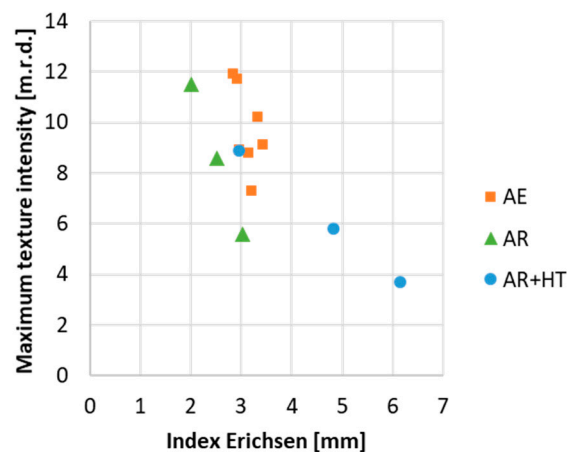


Figure 10. Correlation between texture (maximum intensity of the (0002) pole figure) and Erichsen value for the flat products produced at the different process temperatures: AE (as-extruded T_E : 200–500 °C), AR (as-rolled T_R : 400–500 °C), HT (heat-treated 10 min at 450 °C).

The extruded AZ31 bands (T_E : 200 °C–500 °C) (orange points) have no pronounced dependence of texture or extrusion temperature on Erichsen value (IE) (between 2.8 and 3.6 mm). This finding can be explained by the strong basal alignment and low symmetry in the texture. Due to the strong basal texture (I_{max} : over 8 m.d.r.), dislocations quickly accumulate at the grain boundaries, leading to hardening of the material and eventually to fracture if the stresses are too high. The sheets in the as-rolled condition (green points), T_R : 400 °C–500 °C, show the typical development: decreasing texture intensity, increasing Erichsen value.

The heat-treated AZ31 sheet (blue points) rolled at 400 °C has a very similar IE (3.0 mm) and also a comparable texture intensity (9.1 m.r.d.) to the extruded bands. By increasing the rolling temperature, hence a significant texture weakening after heat treatment (T_R 450 °C: 7.0 m.r.d.; T_R 500 °C: 4.0 m.r.d.), a decrease in strain hardening and a significant increase in Erichsen value occurs (T_R 450 °C: 4.8 mm; T_R 500 °C: 6.1 mm).

Thus, in the case of AZ31, the texture, i.e., the significance of the basal alignment, is the main influencing factor on the biaxial-forming ability and with a reduction in the texture intensity by half, a doubling of the Erichsen value can occur. In addition to texture intensity, the orientation of the grains (tilt angle) naturally also plays a significant role. The AZ31 sheet rolled at 500 °C shows a large grain fraction with basal plane orientation, which is not aligned parallel, to the sheet plane. This crystal orientation also allows sheet thickness reduction by basal slip, thinning along the ND, which without the achievement of increased biaxial formability would not be possible.

5. Conclusions

In this study, rolled and extruded AZ31 flat products were used to show that the determining factors for the textures and microstructures are the deformation and recrystallization mechanisms occurring in the process. Generally, basal slip caused a basal texture component in both massive forming processes. Furthermore, in extrusion, cDRX and prismatic slip at temperatures above 400 °C led to the development of a prismatic component/fiber in the resulting texture. The strong intensity of the textures produced in the extrusion process by DRX was not conducive to high formability (maximum IE (3.4 mm) at 500 °C) and led to a strongly pronounced anisotropy at high extrusion temperatures above

400 °C. During rolling, an increased fraction of compression and tensile twins occurred at high temperatures (here 500 °C). In the subsequent heat treatment, the twins led to a significant weakening of the texture. This enabled a maximum Erichsen value of more than 6 mm to be achieved. Consequently, a high rolling temperature and subsequent SRX were required to improve the formability of the AZ31 sheets.

Author Contributions: Conceptualization and methodology, M.N., G.K., D.L. and J.B.; formal analysis and investigation, M.N.; supervision and validation, K.U.K. and D.L.; writing—original draft preparation, M.N., G.K. and J.B.; writing—review and editing, all authors. All authors have read and agreed to the published version of the manuscript.

Funding: This research received no external funding.

Data Availability Statement: The original data of this study are available from the corresponding author upon reasonable request.

Acknowledgments: The authors would like to thank Alexander Reichart for their help during extrusion and machining of the billets.

Conflicts of Interest: The authors declare no conflict of interest.

References

1. Mordike, B.L.; Ebert, T. Magnesium: Properties—applications—potential. *Mater. Sci. Eng. A-Struct. Mater. Prop. Microstruct. Process.* **2001**, *302*, 37–45. [[CrossRef](#)]
2. Hirsch, J.; Al-Samman, T. Superior light metals by texture engineering: Optimized aluminum and magnesium alloys for automotive applications. *Acta Mater.* **2013**, *61*, 818–843. [[CrossRef](#)]
3. Jiang, M.G.; Xu, C.; Yan, H.; Fan, G.H.; Nakata, T.; Lao, C.S.; Chen, R.S.; Kamado, S.; Han, E.H.; Lu, B.H. Unveiling the formation of basal texture variations based on twinning and dynamic recrystallization in AZ31 magnesium alloy during extrusion. *Acta Mater.* **2018**, *157*, 53–71. [[CrossRef](#)]
4. Jiang, M.G.; Xu, C.; Nakata, T.; Yan, H.; Chen, R.S.; Kamado, S. Rare earth texture and improved ductility in a Mg-Zn-Gd alloy after high-speed extrusion. *Mater. Sci. Eng. A-Struct. Mater. Prop. Microstruct. Process.* **2016**, *667*, 233–239. [[CrossRef](#)]
5. Zeng, Z.R.; Zhu, Y.M.; Xu, S.W.; Bian, M.Z.; Davies, C.H.J.; Birbilis, N.; Nie, J.F. Texture evolution during static recrystallization of cold-rolled magnesium alloys. *Acta Mater.* **2016**, *105*, 479–494. [[CrossRef](#)]
6. Chen, W.Z.; Wang, X.; Kyalo, M.N.; Wang, E.D.; Liu, Z.Y. Yield strength behavior for rolled magnesium alloy sheets with texture variation. *Mater. Sci. Eng. A-Struct. Mater. Prop. Microstruct. Process.* **2013**, *580*, 77–82. [[CrossRef](#)]
7. Stanford, N.; Barnett, M.R. Solute strengthening of prismatic slip, basal slip and {10–12} twinning in Mg and Mg–Zn binary alloys. *Int. J. Plast.* **2013**, *47*, 165–181. [[CrossRef](#)]
8. Blake, A.H.; Caceres, C.H. Solid-solution hardening and softening in Mg–Zn alloys. *Mater. Sci. Eng. A-Struct. Mater. Prop. Microstruct. Process.* **2008**, *483–484*, 161–163. [[CrossRef](#)]
9. Liu, X.; Jonas, J.J.; Li, L.X.; Zhu, B.W. Flow softening, twinning and dynamic recrystallization in AZ31 magnesium. *Mater. Sci. Eng. A-Struct. Mater. Prop. Microstruct. Process.* **2013**, *583*, 242–253. [[CrossRef](#)]
10. Herrera-Solaz, V.; Hidalgo-Manrique, R.; Perez-Prado, M.T.; Letzig, D.; Llorca, J.; Segurado, J. Effect of rare earth additions on the critical resolved shear stresses of magnesium alloys. *Mater. Lett.* **2014**, *128*, 199–203. [[CrossRef](#)]
11. Baczmanski, A.; Wronski, M.; Kot, P.; Wronski, S.; Labaza, A.; Wierzbowski, K.; Ludwik, A.; Marciszko-Wiackowska, M. The role of basal slip in the generation of intergranular stresses in magnesium alloy studied using X-ray diffraction and modelling. *Mater. Des.* **2021**, *202*, 109543. [[CrossRef](#)]
12. Koike, J.; Kobayashi, T.; Mukai, T.; Watanabe, H.; Suzuki, M.; Maruyama, K.; Higashi, K. The activity of non-basal slip systems and dynamic recovery at room temperature in fine-grained AZ31B magnesium alloys. *Acta Mater.* **2003**, *51*, 2055–2065. [[CrossRef](#)]
13. Klaumünzer, D.; Hernandez, J.V.; Yi, S.; Letzig, D.; Kim, S.-H.; Kim, J.J.; Seo, M.H.; Ahn, K. *Magnesium Process and Alloy Development for Applications in the Automotive Industry*; Magnesium Technology 2019; Joshi, V.V., Jordon, J.B., Orlov, D., Neelameggham, N.R., Eds.; Springer International Publishing: Cham, Switzerland, 2019; pp. 15–20.
14. Xu, Y.Z.; Li, J.Y.; Qi, M.F.; Liao, L.H.; Gao, Z.J. Enhanced mechanical properties of Mg–Zn–Y–Zr alloy by low-speed indirect extrusion. *J. Mater. Res. Technol.* **2020**, *9*, 9856–9867. [[CrossRef](#)]
15. Jain, A.; Duygulu, O.; Brown, D.W.; Tome, C.N.; Agnew, S.R. Grain size effects on the tensile properties and deformation mechanisms of a magnesium alloy, AZ31B, sheet. *Mater. Sci. Eng. A-Struct. Mater. Prop. Microstruct. Process.* **2008**, *486*, 545–555. [[CrossRef](#)]
16. Gottstein, G.; Al Samman, T. Texture development in pure Mg and Mg alloy AZ31. *Mater. Sci. Forum* **2005**, *495–497*, 623–632. [[CrossRef](#)]
17. Yi, S.B.; Brokmeier, H.G.; Letzig, D. Microstructural evolution during the annealing of an extruded AZ31 magnesium alloy. *J. Alloys Compd.* **2010**, *506*, 364–371. [[CrossRef](#)]

18. Styczynski, A.; Hartig, C.; Bohlen, J.; Letzig, D. Cold rolling textures in AZ31 wrought magnesium alloy. *Scr. Mater.* **2004**, *50*, 943–947. [[CrossRef](#)]
19. Jeong, H.T.; Ha, T.K. Texture development in a warm rolled AZ31 magnesium alloy. *J. Mater. Process. Technol.* **2007**, *187*, 559–561. [[CrossRef](#)]
20. Bohlen, J.; Wendt, J.; Nienaber, M.; Kainer, K.U.; Stutz, L.; Letzig, D. Calcium and zirconium as texture modifiers during rolling and annealing of magnesium-zinc alloys. *Mater. Charact.* **2015**, *101*, 144–152. [[CrossRef](#)]
21. Farzadfar, S.A.; Martin, E.; Sanjari, M.; Essadiqi, E.; Yue, S. Texture weakening and static recrystallization in rolled Mg-2.9Y and Mg-2.9Zn solid solution alloys. *J. Mater. Sci.* **2012**, *47*, 5488–5500. [[CrossRef](#)]
22. Imandoust, A.; Barrett, C.D.; Al-Samman, T.; Inal, K.A.; El Kadiri, H. A review on the effect of rare-earth elements on texture evolution during processing of magnesium alloys. *J. Mater. Sci.* **2016**, *52*, 1–29. [[CrossRef](#)]
23. Nienaber, M.; Yi, S.; Kainer, K.U.; Letzig, D.; Bohlen, J. On the Direct Extrusion of Magnesium Wires from Mg-Al-Zn Series Alloys. *Metals* **2020**, *10*, 1208. [[CrossRef](#)]
24. Shahzad, M.; Wagner, L. Influence of extrusion parameters on microstructure and texture developments, and their effects on mechanical properties of the magnesium alloy AZ80. *Mater. Sci. Eng. A-Struct. Mater. Prop. Microstruct. Process.* **2009**, *506*, 141–147. [[CrossRef](#)]
25. Javaid, A.; Czerwinski, F. Effect of hot rolling on microstructure and properties of the ZEK100 alloy. *J. Magnes. Alloy.* **2019**, *7*, 27–37. [[CrossRef](#)]
26. Guo, F.; Zhang, D.F.; Yang, X.S.; Jiang, L.Y.; Chai, S.S.; Pan, F.S. Effect of rolling speed on microstructure and mechanical properties of AZ31 Mg alloys rolled with a wide thickness reduction range. *Mater. Sci. Eng. A-Struct. Mater. Prop. Microstruct. Process.* **2014**, *619*, 66–72. [[CrossRef](#)]
27. Sanjari, M.; Kabir, A.S.H.; Farzadfar, A.; Utsunomiya, H.; Petrov, R.; Kestens, L.; Yue, S. Promotion of texture weakening in magnesium by alloying and thermomechanical processing. II: Rolling speed. *J. Mater. Sci.* **2013**, *49*, 1426–1436. [[CrossRef](#)]
28. Huang, X.S.; Suzuki, K.; Chino, Y.; Mabuchi, M. Influence of initial texture on rolling and annealing textures of Mg-3Al-1Zn alloy sheets processed by high temperature rolling. *J. Alloys Compd.* **2012**, *537*, 80–86. [[CrossRef](#)]
29. Jin, L.; Dong, J.; Wang, R.; Peng, L.M. Effects of hot rolling processing on microstructures and mechanical properties of Mg-3%Al-1%Zn alloy sheet. *Mater. Sci. Eng. A* **2010**, *527*, 1970–1974. [[CrossRef](#)]
30. Bohlen, J.; Yi, S.B.; Letzig, D.; Kainer, K.U. Effect of rare earth elements on the microstructure and texture development in magnesium-manganese alloys during extrusion. *Mater. Sci. Eng. A-Struct. Mater. Prop. Microstruct. Process.* **2010**, *527*, 7092–7098. [[CrossRef](#)]
31. Zhang, B.P.; Geng, L.; Huang, L.J.; Zhang, X.X.; Dong, C.C. Enhanced mechanical properties in fine-grained Mg-1.0Zn-0.5Ca alloys prepared by extrusion at different temperatures. *Scr. Mater.* **2010**, *63*, 1024–1027. [[CrossRef](#)]
32. Zeng, Z.; Stanford, N.; Davies, C.H.J.; Nie, J.-F.; Birbilis, N. Magnesium extrusion alloys: A review of developments and prospects. *Int. Mater. Rev.* **2018**, *64*, 27–62. [[CrossRef](#)]
33. Meza-Garcia, E.; Bohlen, J.; Yi, S.; Letzig, D.; Krausel, V.; Landgrebe, D.; Kainer, K.U. Influence of alloying elements and extrusion process parameter on the recrystallization process of Mg-Zn alloys. *Mater. Today-Proc.* **2015**, *2*, S19–S25. [[CrossRef](#)]
34. Kurz, G.; Nienaber, M.; Bohlen, J.; Letzig, D.; Kainer, K.U. *Variation of Extrusion Process Parameter for the Magnesium Alloy ME21*; Springer International Publishing: Cham, Switzerland, 2020; pp. 181–188.
35. Isakovic, J.; Bohlen, J.; Ben Khalifa, N.; Kainer, K.U. Microstructure Development of Magnesium Alloys AZ31 and AZ80 Due to Temperature Evolution during Direct Extrusion. In Proceedings of the International Aluminum Extrusion Technology, Orlando, FL, USA, 2022.
36. Nienaber, M.; Kainer, K.U.; Letzig, D.; Bohlen, J. Processing Effects on the Formability of Extruded Flat Products of Magnesium Alloys. *Front. Mater.* **2019**, *6*, 253. [[CrossRef](#)]
37. Hantzsche, K.; Bohlen, J.; Wendt, J.; Kainer, K.U.; Yi, S.B.; Letzig, D. Effect of rare earth additions on microstructure and texture development of magnesium alloy sheets. *Scr. Mater.* **2010**, *63*, 725–730. [[CrossRef](#)]
38. Bohlen, J.; Chmelik, F.; Dobron, P.; Kaiser, F.; Letzig, D.; Lukac, P.; Kainer, K.U. Orientation effects on acoustic emission during tensile deformation of hot rolled magnesium alloy AZ31. *J. Alloys Compd.* **2004**, *378*, 207–213. [[CrossRef](#)]
39. Huang, X.; Suzuki, K.; Saito, N. Textures and stretch formability of Mg-6Al-1Zn magnesium alloy sheets rolled at high temperatures up to 793K. *Scr. Mater.* **2009**, *60*, 651–654. [[CrossRef](#)]
40. Huang, X.S.; Suzuki, K.; Chino, Y.; Mabuchi, M. Improvement of stretch formability of Mg-3Al-1Zn alloy sheet by high temperature rolling at finishing pass. *J. Alloys Compd.* **2011**, *509*, 7579–7584. [[CrossRef](#)]
41. Agnew, S.R.; Duygulu, O. Plastic anisotropy and the role of non-basal slip in magnesium alloy AZ31B. *Int. J. Plast.* **2005**, *21*, 1161–1193. [[CrossRef](#)]
42. Ion, S.E.; Humphreys, F.J.; White, S.H. Dynamic Recrystallization and the Development of Microstructure during the High-Temperature Deformation of Magnesium. *Acta Metall.* **1982**, *30*, 1909–1919. [[CrossRef](#)]
43. Dudamell, N.V.; Ulacia, I.; Galvez, F.; Yi, S.; Bohlen, J.; Letzig, D.; Hurtado, I.; Perez-Prado, M.T. Twinning and grain subdivision during dynamic deformation of a Mg AZ31 sheet alloy at room temperature. *Acta Mater.* **2011**, *59*, 6949–6962. [[CrossRef](#)]
44. Barnett, M.R. Twinning and the ductility of magnesium alloys Part I: “Tension” twins. *Mater. Sci. Eng. A* **2007**, *464*, 1–7. [[CrossRef](#)]
45. Barnett, M.R. Twinning and the ductility of magnesium alloys. *Mater. Sci. Eng. A* **2007**, *464*, 8–16. [[CrossRef](#)]

46. Jain, A.; Agnew, S.R. Modeling the temperature dependent effect of twinning on the behavior of magnesium alloy AZ31B sheet. *Mater. Sci. Eng. A-Struct. Mater. Prop. Microstruct. Process.* **2007**, *462*, 29–36. [[CrossRef](#)]
47. Huang, X.S.; Suzuki, K.; Watazu, A.; Shigematsu, I.; Saito, N. Effects of thickness reduction per pass on microstructure and texture of Mg-3Al-1Zn alloy sheet processed by differential speed rolling. *Scr. Mater.* **2009**, *60*, 964–967. [[CrossRef](#)]
48. Azghandi, S.H.M.; Weiss, M.; Arhatari, B.D.; Adrien, J.; Maire, E.; Barnett, M.R. A rationale for the influence of grain size on failure of magnesium alloy AZ31: An in situ X-ray microtomography study. *Acta Mater.* **2020**, *200*, 619–631. [[CrossRef](#)]
49. Victoria-Hernandez, J.; Yi, S.; Klaumunzer, D.; Letzig, D. Recrystallization behavior and its relationship with deformation mechanisms of a hot rolled Mg-Zn-Ca-Zr alloy. *Mater. Sci. Eng. A-Struct. Mater. Prop. Microstruct. Process.* **2019**, *761*, 138054. [[CrossRef](#)]
50. Basu, I.; Al-Samman, T. Hierarchical Twinning Induced Texture Weakening in Lean Magnesium Alloys. *Front. Mater.* **2019**, *6*, 187. [[CrossRef](#)]
51. Perez-Prado, M.T.; del Valle, J.A.; Contreras, J.M.; Ruano, O.A. Microstructural evolution during large strain hot rolling of an AM60 Mg alloy. *Scr. Mater.* **2004**, *50*, 661–665. [[CrossRef](#)]
52. Dillamore, I.L.; Hadden, P.; Stratford, D.J. Texture Control and the Yield Anisotropy of Plane Strain Magnesium Extrusions. *Texture* **1972**, *1*, 17–29. [[CrossRef](#)]
53. Gall, S.; Mueller, S.; Reimers, W. Extrusion of AZ31 Magnesium Sheet. *Mater. Sci. Forum* **2010**, *638–642*, 1530–1534. [[CrossRef](#)]
54. Bhattacharyya, J.J.; Agnew, S.R.; Muralidharan, G. Texture enhancement during grain growth of magnesium alloy AZ31B. *Acta Mater.* **2015**, *86*, 80–94. [[CrossRef](#)]
55. Steiner, M.A.; Bhattacharyya, J.J.; Agnew, S.R. The origin and enhancement of {0001}<112-0> texture during heat treatment of rolled AZ31B magnesium alloys. *Acta Mater.* **2015**, *95*, 443–455. [[CrossRef](#)]
56. Agnew, S.R.; Yoo, M.H.; Tome, C.N. Application of texture simulation to understanding mechanical behavior of Mg and solid solution alloys containing Li or Y. *Acta Mater.* **2001**, *49*, 4277–4289. [[CrossRef](#)]
57. Imandoust, A.; Barrett, C.D.; Al-Samman, T.; Tschopp, M.A.; Essadiqi, E.; Hort, N.; El Kadiri, H. Unraveling Recrystallization Mechanisms Governing Texture Development from Rare-Earth Element Additions to Magnesium. *Metall. Mater. Trans. A-Phys. Metall. Mater. Sci.* **2018**, *49*, 1809–1829. [[CrossRef](#)]
58. Tang, T.; Shao, Y.C.; Li, D.Y.; Peng, L.M.; Peng, Y.H.; Zhang, S.R.; Wu, P.D. Polycrystal plasticity simulation of extrusion of a magnesium alloy round bar: Effect of strain path non-uniformity. *J. Alloys Compd.* **2018**, *730*, 161–181. [[CrossRef](#)]
59. Fatemi-Varzaneh, S.M.; Zarei-Hanzaki, A.; Beladi, H. Dynamic recrystallization in AZ31 magnesium alloy. *Mater. Sci. Eng. A* **2007**, *456*, 52–57. [[CrossRef](#)]
60. Bohlen, J.; Nurnberg, M.R.; Senn, J.W.; Letzig, D.; Agnew, S.R. The texture and anisotropy of magnesium-zinc-rare earth alloy sheets. *Acta Mater.* **2007**, *55*, 2101–2112. [[CrossRef](#)]